1. Theodorovic, S., *Nature*, 1963, **197**, 86–87.
2. Moss, G. D., *Parasitology*, 1972, **64**, 311–320.
3. Terry, R. and Hudson, K., in *Immune Reactions to Parasites* (ed. Frank, W.), Gustav Fischer Verlag, New York, 1982, pp. 125–139.
4. Price, T. and Turner, K. J., *Int. J. Parasitol.*, 1986, **16**, 607–615.
5. Hermanek, J. J., *Helminthology*, 1991, **65**, 121–132.
6. Yoshimura, K., Sugaya, H., Ishida, K., Khan, W. I., Abe, T. and Unno, K., *Int. J. Parasitol.*, 1993, **23**, 997–1003.
7. Cox, P. E. G., *Nature*, 1978, **273**, 623–626.
8. Hopkins, C. A., Subrahmanian, G. and Stallard, H., *Parasitology*, 1972, **65**, 111–120.
9. Dissanaike, A. S. and Mak, J. W., *J. Helminthol.*, 1980, **54**, 117–122.
10. Cross, J. H., Partono, F., Hsu, M. K., Ash, L. R. and Oemijati, S., *Am. J. Trop. Med. Hyg.*, 1979, **28**, 56–66.
11. Fatma, N., Sharma, S. and Chatterjee, R. K., *Acta Tropica*, 1989, **216**, 311–321.
12. Chatterjee, R. K., Fatma, N., Murthy, P. K., Sinha, P., Kulshrestha, D. K. and Dhawan, B. N., *Drug Dev. Res.*, 1992, **26**, 67–78.
13. Worms, M. J., Terry, R. J. and Terry, A. J., *Parasitology*, 1961, **47**, 963–970.
14. Singh, D. P., Misra, S. and Chatterjee, R. K., *Indian J. Exp. Biol.*, 1988, **26**, 48–52.
15. Bhatia, A., Agarwal, A. and Vinayak, V. K., *Indian J. Med. Res.*, 1981, **74**, 506–511.
16. Saxena, K. C., Puri, A., Sumati, Saxena, R. and Saxena, R. P., *Immun. Invest.*, 1991, **20**, 431–435.
17. Burleigh, I. G. and Schmike, R. T., *Biochem. Biophys. Res. Commun.*, 1968, **31**, 831–836.
18. Wang, E. J. and Saz, H. J., *J. Parasitol.*, 1974, **60**, 316–321.
19. Barker, B. S. and Summerson, W. H., *J. Biol. Chem.*, 1941, **138**, 535–554.
20. Melvin, M., Ketchel, Cutting, B., Favour, M. D. and Sturgis, S. H., *J. Exp. Med.*, 1958, **107**, 211–218.
21. Nielsen, K., Fogh, L. and Anderson, S., *Acta Pathol. Microbiol. Scand.*, 1974, **82**, 919–920.
22. Pollaco, S., Nicholas, W. L., Mitchell, G. F. and Stewart, A. C., *Int. J. Parasitol.*, 1978, **8**, 457–462.
23. Lammas, D. A., Mitchell, L. A. and Waklein, D., *Parasite Immunol.*, 1987, **9**, 951–601.
24. Letonja, T., Hammerberg, C., Davis, S. and Hammerberg, B., *J. Parasitol.*, 1988, **74**, 985–992.
25. Renoux, G. and Renoux, M., *Clinical Immunol. Immunopathol.*, 1980, **15**, 23–32.
26. Lammler, G., *Pestic Sci.*, 1977, **8**, 563–567.

ACKNOWLEDGEMENTS. N. F. and A. S. D. thank CSIR, New Delhi, for financial assistance. We are grateful to Dr V. M. L. Srivastava, CDRI, Lucknow, for his help in conducting metabolic study of parasites.

Received 10 June 1996; revised accepted 4 February 1997

Block rotation in a part of eastern Dharwar craton of South India – A suggestion from aeromagnetic data interpretation

Ch. Rama Rao, D. S. Bhaskara Rao and D. Atchuta Rao

National Geophysical Research Institute, Hyderabad 500 007, India

Deformation in the brittle part of the earth's crust often gives rise to faults. It is believed that these faults tend to form conjugate fracture systems, and the rigid crustal blocks bounded by these fractures rotate about horizontal axes in the event of dip slip and about a vertical axis in the strike slip environment. Recent studies in the granite–greenstone terrain of a part of eastern Dharwar craton in South India (3.4–2.5 Ga) have suggested a tectonic environment in which the cross cutting NW, NE and ENE trending faults systems divided the crust into a mosaic of rigid crustal blocks which might have been rotated. Analysis of the aeromagnetic data of a part of this area suggests that (i) the NW–SE trending shears have strike-slip component, (ii) the rigid crustal blocks have rotated through an angle of 8.5° clockwise and (iii) the depth of the decoupling zone beneath the strike-slip faults is estimated to be 3.0 km, i.e. it is in the upper crustal level.

UNDER a variety of tectonic conditions the brittle part of the earth's crust is often prone to deformation. This deformation generally gives rise to faults. Simultaneous translation and rotation of fault-bounded crustal fragments, which are governed by kinematic constraints, are widely reported in varied geological and tectonic settings[1–4]. Fault-bounded crustal blocks rotate about vertical axes, where a fault slip has a strike parallel component[1,5,6], and on horizontal axes where dip slip occurs. Faults also rotate under continued deformation. These block rotations may occur (i) in discrete shear zones, (ii) zones of distributed shear probably caused by oblique subduction, (iii) during accretion, (iv) due to oroclinal bending, and (v) in overthrust faulting[2]. Such rotation may take place in different scales, starting from an outcrop to regional scale[5,7,8]. Recent studies on the granite–greenstone terrain of a part of Eastern Dharwar craton of south India, based on Landsat, aerial photos, age relationships of the structures such as faults, lineaments, dykes, etc. and on field evidences, suggested that tectonically this area is a composite mosaic of crustal blocks of various dimensions. These have rotated about vertical axes in geological time in response to various tectonic processes[9]. Several workers have reported palaeomagnetic, seismic and structural evidences in support of block rotation[2,4,10–17].

The angles through which the blocks can rotate are, in some cases 15–20°, and in some other cases the horizontal rotations are reported to be 70° and even more between the two parallel faults in strike slip environment.

Aeromagnetic data and its interpretation can be utilized for (i) geological mapping, (ii) spotting of mineralized zones, and (iii) unravelling of structural elements like fault/shear zones, dyke swarms, and their alignments and extensions, boundaries of basinal and domal features. Aeromagnetic data can also be used to identify strike slip movements, rotational patterns, etc. and help in deriving basement configurations, thereby in the understanding of the structural evolution of different crustal domains. Here, we present a structural and tectonic scenario, derived from the interpretation of a small portion of the aeromagnetic data to look for terrains suggesting block rotation.

The study area forms a small portion of the granite greenstone terrain in Eastern Dharwar craton situated to the west of the Proterozoic Cuddapah basin. This area is bounded by 14°25′0″ and 14°35′0″N lat., and 77°30′0″ and 77°55′0″E long. (Figure 1 *a*).

The Archaean granite–greenstone terrain west of the proterozoic Cuddapah basin is a low to medium grade terrain, consisting of steeply dipping green schist belts, often invaded by highly elongated 'granitoid bodies'. The terrain is traversed by NW, NE and ENE trending Precambrian dykes[18]. Dykes of younger ages traversing in other directions are also there. Quartz reefs are mostly emplaced along NW trending shear zones in this part of the area. A comprehensive geological history of this area is provided by Raju *et al.*[19]. The aeromagnetic lineaments in this area mostly represent dyke systems and fault domains. Two NW–SE trending parallel fault/shear zones, viz. the Hampapuram and Kandukuru faults (Figure 1 *b*) are cut by ENE trending faults, often occupied by ENE trending dykes. Quartz reefs are emplaced in both the fault/shear zones. Cataclastic and brecciated rock matrix are present in these two fault/shear zones. Displacement of dykes indicates a possible right lateral movement along the faults[9]. The aeromagnetic data for this belt has been reprocessed to infer structures, if any, related to the faults/shears and to bring out the tectonic history *vis-à-vis* the proposed block rotation hypothesis.

The National Geophysical Research Institute (NGRI) in collaboration with the Geological Survey of India (GSI) carried out an airborne magnetic survey for mineral exploration during 1980–82 over a part of the Eastern Dharwar craton and part of the Proterozoic Cuddapah basin, at a flight height of 150 m with a flight line spacing of 0.5 km in some selected areas and with a line spacing of 1 km in most of the area. The area under study (Figure 1 *a*) forms a small part of the aeromagnetic map on the Archaean basement complex.

The total intensity aeromagnetic anomaly field data of the study area have been reprocessed, and high-pass and low-pass filtered anomaly maps have been prepared using the MAGMAP software of Paterson, Grant and Watson Ltd., Canada. Reduced to equator (RTE) option has been applied on the above high-pass and low-pass filtered maps. These are shown in Figures 2 *a* and 3 *a* respectively. This option has been preferred because: (i) the high-pass filtering accentuates the shallow magnetic features at the expense of the broader and deep-seated sources, and allows one to identify easily the various shallow magnetic trends, (ii) the centres of the magnetic lows and/or highs in the RTE map clearly locate the tops of the sources. The low-pass filtered RTE map has been analysed to identify the possible downward continuity of the shallow structural features.

Aeromagnetic interpretation helps in recognizing long linear features like faults/shears, dykes and other structural lineaments. Offsets in continuity of the magnetic

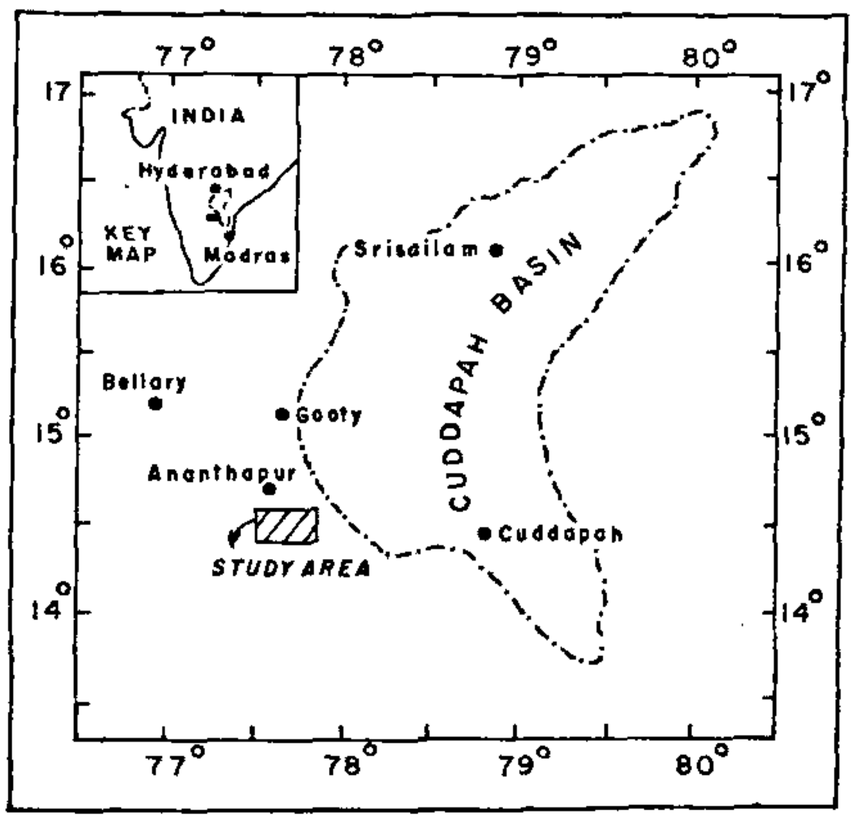

Figure 1 *a*. Location map of the study area.

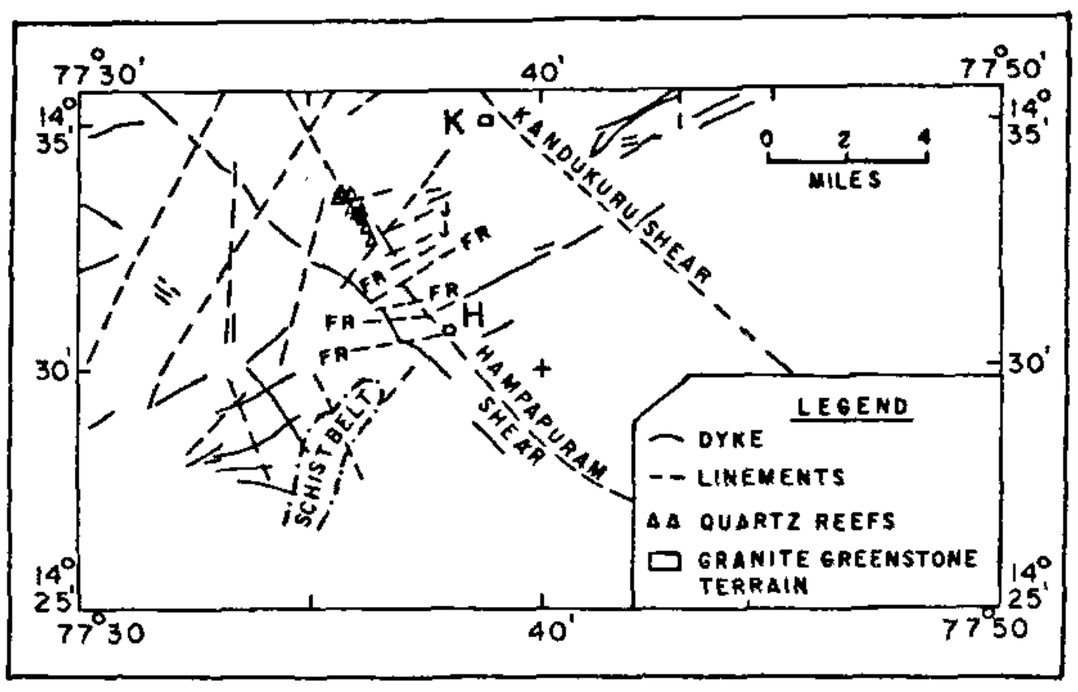

Figure 1 *b*. Geological map of the study area.

trends/lineaments, abrupt terminations of magnetic lows and/or highs, drag features, contour nosings, alignments of lows or highs, etc. are some of the direct indicators of fault/shear zones[20]. A persistent offset in the magnetic trends and drag features on either side of a fault/shear zone indicates the possibility of strike slip environment, even though large scale strike slip faults do not leave any morphological evidence for strike slip faulting.

The low geomagnetic latitudes such as the present area, an intensely sheared tectonic zone with a possibility of depletion and/or destruction of magnetic minerals occurring, can be identified by the characteristic positive magnetic anomaly closures all along the shear zone.

Using the above criteria, the aeromagnetic anomaly map of this area has been interpreted and lineaments, dislocation planes, possible shear/faults, etc. identified. The interpreted structures are shown in Figures 2 *b* and 3 *b*.

Two major structural elements that are dominant and striking on the map are the NW–SE trending Hampapuram fault/shear in the west and the Kandukuru fault/shear in the east. A number of ENE and EW trending magnetic lineaments, mostly representing fault/shear zones, often occupied by dykes, are also seen cutting across the NW features, thus forming a domain of fault system. The NNE–SSW trending magnetic anomaly feature represents the extended portion of the Hagari–Ramgiri schist belt. A general observation is that there are fault zones both in the north and south bounding the Hampapuram and the Kandukuru fault/shear zones. The ENE and EW features are found to have been offset by the NW faults. The extent of offsets are shown as d1, d2, d3, . . . in Figure 2 *b*.

Shifts in the NE and ENE trending magnetic anomaly

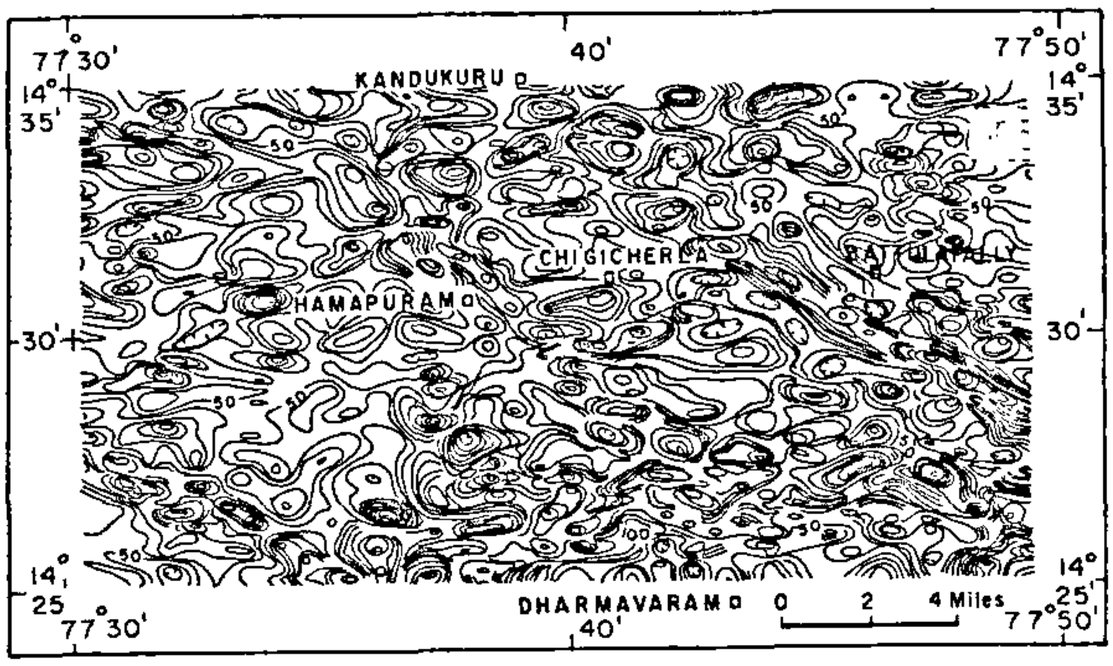

Figure 2 *a*. High-pass filtered, reduced to equator total intensity aeromagnetic anomaly map of the area (cont. interval 10 nT).

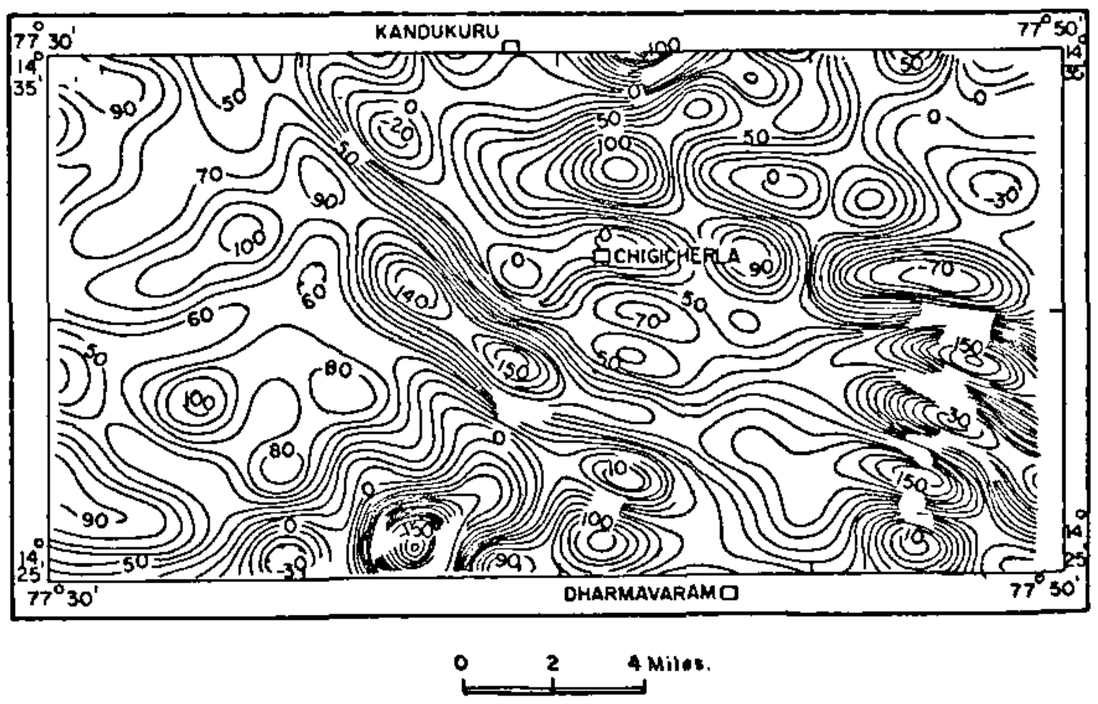

Figure 3 *a*. Low-pass filtered, reduced to equator total intensity aeromagnetic anomaly map.

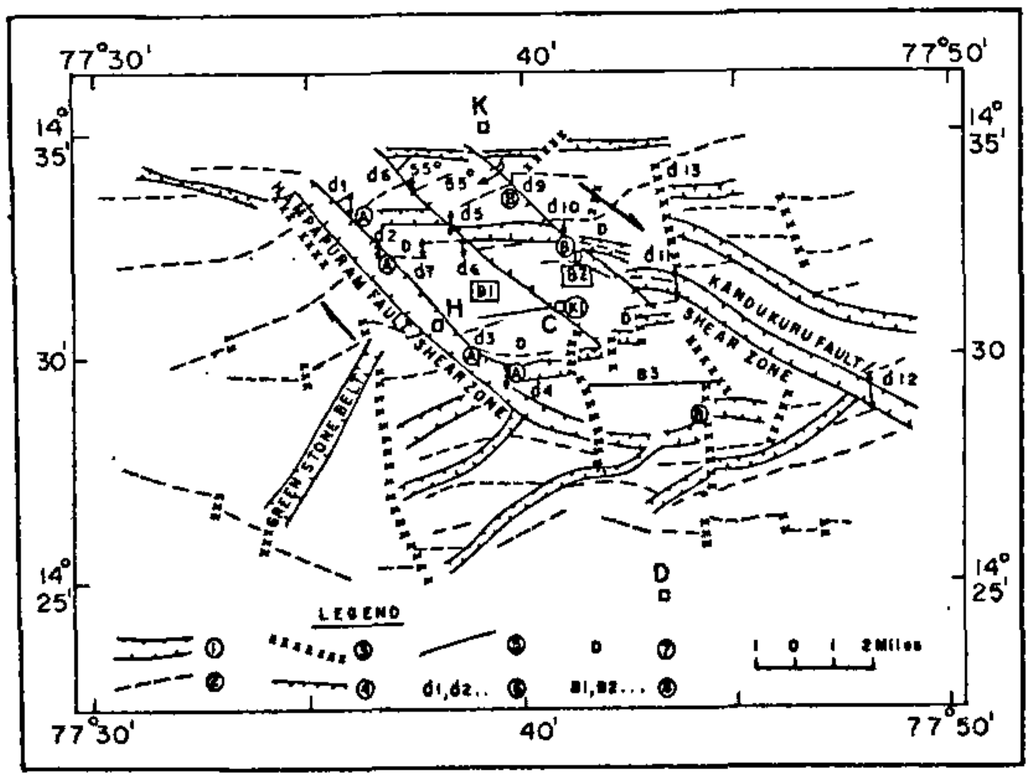

Figure 2 *b*. Structural interpretation map of the high-pass filtered, reduced to equator total intensity anomaly map of the area. 1. Positive closures indicate fault/shear; 2. NE and ENE trending magnetic lineaments; 3. Dislocation planes; 4. Possible fault traces within the block; 5. Inferred extensional fractures; 6. Extent of displacements along shears; 7. Drag features indicate strike slip movement; 8. Inferred rigid crustal blocks bounded by shears.

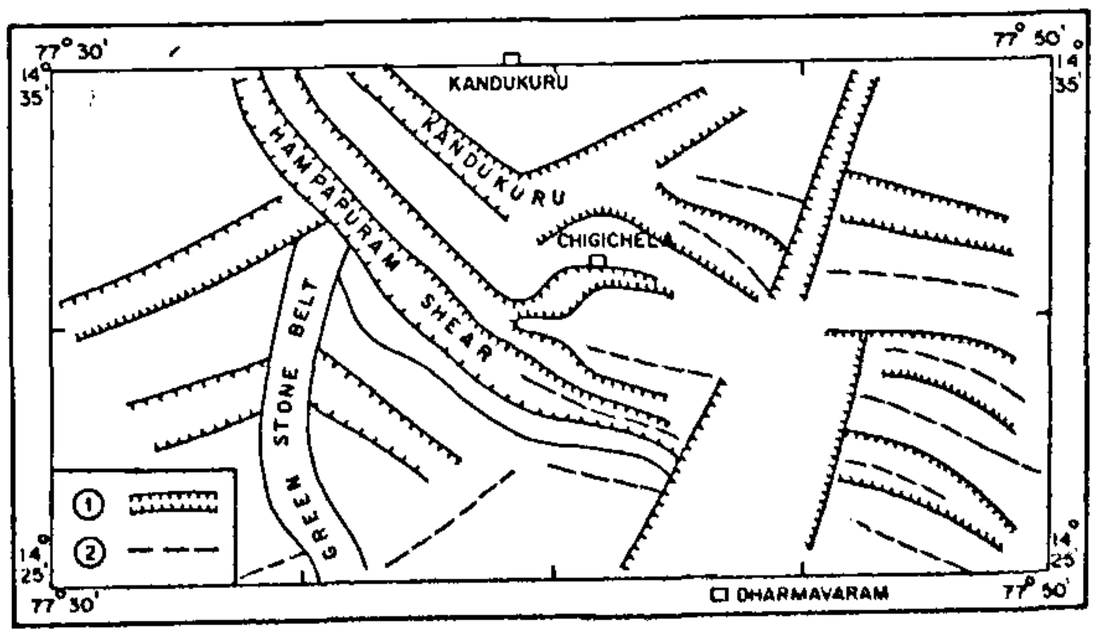

Figure 3 *b*. Structural interpretation map of the low-pass filtered, reduced to equator total intensity aeromagnetic anomaly map of the area. Note the existence of both the Hampapuram and Kandukuru fault/shear even at deeper levels.

trends (Figure 2 *b*), designated as 'A' on either side of the NW–SE trending Hampapuram fault and 'B' on either side of the Kandukuru shear zone and the drag features 'D', indicate strike slip movement. These shifts in the anomalies can be attributed to a right lateral movement along the shear zones. Field and other evidences also confirm right lateral movement in regional scale[9]. The positive magnetic anomaly closures as shown in the figure, are associated with intense shearing. Continued tectonic activity in this part of the craton has resulted in a sygmoidal shearing as well as rotational features in the faults (as indicated by arrows in the Figure 2 *b*). Thus, interpretation of this map led us to identify rigid crustal blocks B1, B2 and B3 bounded on all sides by strike slip faults which probably caused the blocks to rotate. Occurrence of kimberlite intrusion at one of the corners in the blocks B1 (shown as k1) seems to have been owing to a possible extension due to rotation in this corner. A clockwise rotation of the blocks owing to the strike slip is envisaged in this part.

Figure 3 *b* is the structural interpretation map of the low-pass filtered, reduced to equator data. This interpretation further supports the continuation of the two shear zones vertically downwards. The log normalized radially averaged power spectrum (Figure 4 *a*) computed for the low-pass filtered map gives an average depth of 3.0 km for a possible magnetic marker horizon. This depth, perhaps, represents the depth to a mid-crustal disharmony beneath the strike slip fault system[21]. Thus, geophysical inferences suggest a region of block rotation

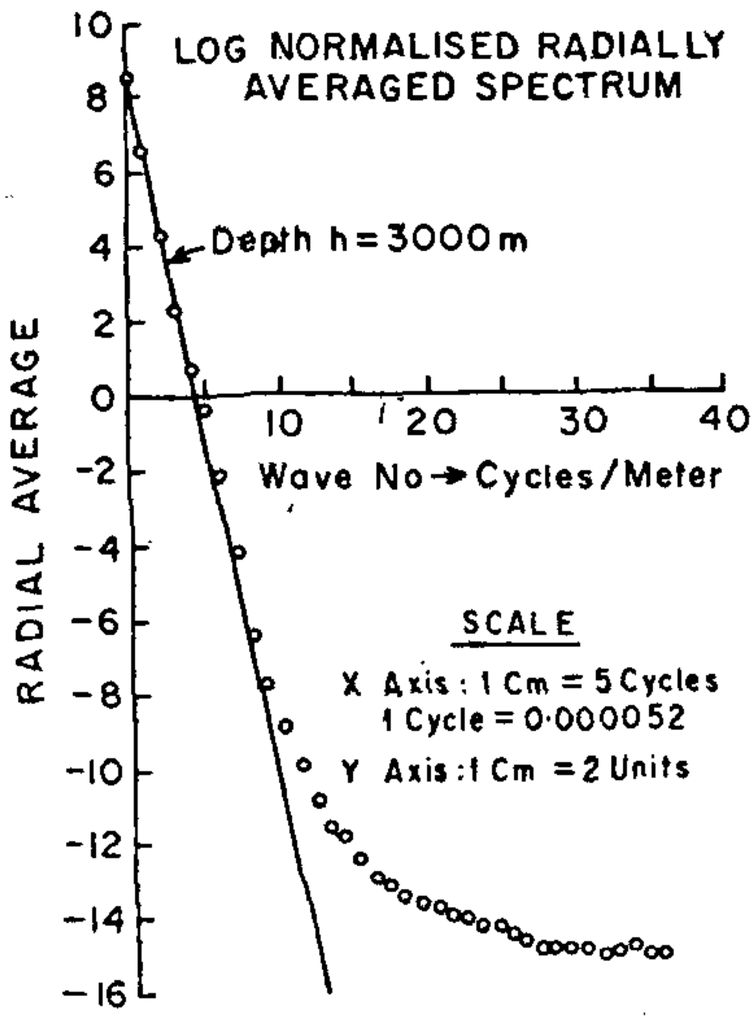

Figure 4 *a*. Log-normalized radially averaged power spectrum computed for the low-pass filtered aeromagnetic anomaly field data. $h = 3$ km. possibly indicates the depth to the mid-crustal disharmony beneath the hears.

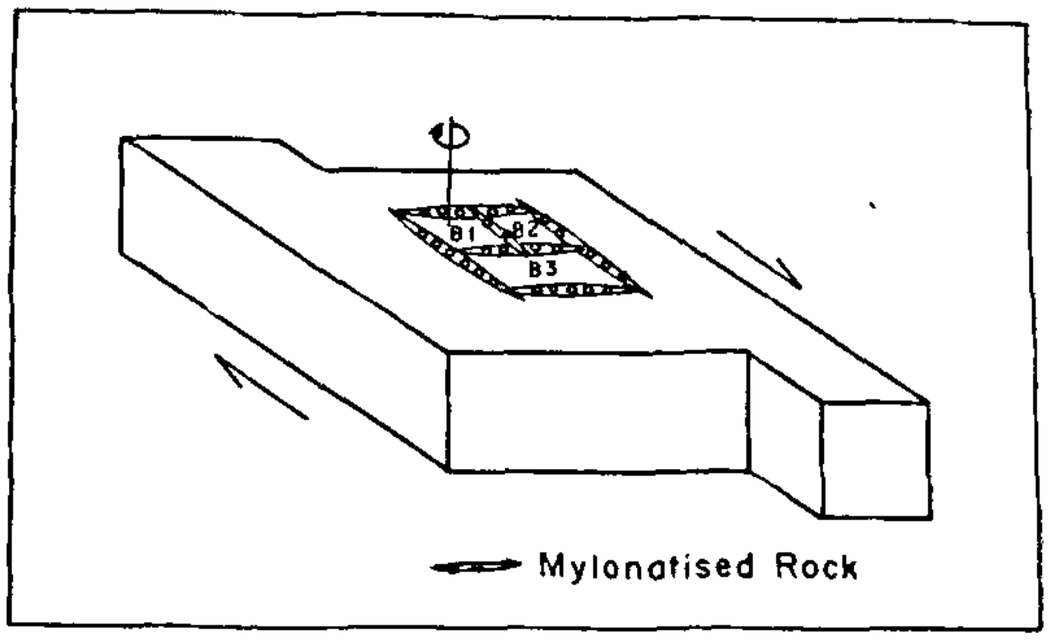

Figure 4 *b*. Interpreted block diagram showing the inferred crustal blocks B1, B2 and B3 surrounded by the cataclastic and brecciated rock matrix.

in which the blocks are surrounded by deformed rock matrix. Based on these structural inferences, a block diagram showing the possible strike-slip and block rotation in this region is presented in Figure 4 *b*.

An attempt is made here to calculate the angle of block rotation using the relation given by Nur *et al.*[22]

$$d = W \sin\phi \, [\sin\alpha \times \sin(\alpha - \phi)]^{-1}, \qquad (1)$$

where d is the displacement along the fault, W the width of the faulted block, α the initial angle between the faults and the boundary of the domain and ϕ the block rotation angle.

The displacement d is measured from the interpreted section. The average of the horizontal displacements on either side of each fault (here the displacements $d1$, $d2$, etc. between A's B's on either side of the faults) represents the strike-slip displacement along the faults.

The initial angle is the angle between the fault and the boundary as shown in the figure, and the width w is the average distance between the two faults.

Here $d = 680$ m (average displacement), $w = 3165$ m (Block 1), $w = 2850$ m (Block 2).

Substituting these values from the interpreted section, the angle ϕ is calculated from equation (1) and is 9.0 and 8.0 degrees clockwise for blocks 1 and 2 respectively.

Interpretation of a part of aeromagnetic data from a region of strike-slip movement in a Precambrian granite greenstone terrain, has resulted in identifying a zone of possible block rotation. The average angle of block rotation is determined from the width w, initial angle α and the displacement d measured from the interpreted map, using the relation given by Nur *et al.*[22] and is 8.5 degrees clockwise. Computation of the radial power spectrum from the low-pass filtered aeromagnetic anomaly data of this area, has given an average depth to a possible magnetic marker horizon at a depth of 3.0 km. This probably represents the depth to the decoupling zone in the upper crustal level below the shear zone.

1. Freund, R., *J. Geol.*, 1970, **78**, 188–200.
2. Beck, M. E. Jr., *Am. J. Sci.*, 1976, **276**, 694–712; Beck, M. E. Jr., *Palaeomagnetic Rotations and Continental Deformation*, Kluwer Academic Publishers, Dodrecht, 1989.
3. Luyendyk, B. P., Kamerling, M. J. and Terres, R. R., *Geol. Soc. Am. Bull.*, 1980, **91**, 211–217.
4. Ron, H., Aydin, A. and Nur, A., *Geology*, 1986, **14**, 1020–1023.
5. Freund, R., *Tectonophysics*, 1974, **21**, 93–194.
6. Garfunkel, Z., *Geol. Soc. Am. Bull.*, 1974, **85**, 1931–1944.
7. Carey, S. W., *Continental Drift*, University of Tasmania Press, 1955.
8. Ramsay, J. G., *J. Geol.*, 1961, **69**, 84.
9. Chetty, T. R. K., *J. Geodynamics*, 1995, **20**, 255–266.
10. Cox, A., *Nature*, 1957, **179**, 685–686.
11. Norris, D. K. and Black, R. F., *Nature*, 1961, **192**, 933–935.
12. Barger, W. B. A. and Robertson, W. A., *Can. J. Earth Sci.*, 1973, **10**, 1519–1532.
13. Nur, A. and Helsley, C. E., *Earth Planet. Sci. Lett.*, 1971, **10**, 376–379.
14. Fagin, S. W. and Gose, W. A., *Geology*, 1983, **11**, 505–508.
15. Ron, H., Freund, R., Garfunkel, Z. and Nur, A., *J. Geophys. Res.*, 1984, **89**, 6256–6270.
16. Terres, R. R. and Luyendyk, B. P., *J. Geophys. Res.*, 1985, **90**, 12467–12484.
17. Wells, R. E. and Coe, R. S., *J. Geophys. Res.*, 1985, **90**, 1925–1947.
18. Murthy, Y. G. K., Babu Rao, V., Guptasarma, D., Rao, J. M., Rao, M. N. and Bhattacharji, S., *Mafic Dike Swarms* (eds Hall, H. E. and Fabrig, W. F.), 1987, pp. 303–316.
19. Raju, K. C. C., Karimuddin, Md. and Prabhakara Rao, P., *Geol. Surv. India*, 1970, **47**, 54.
20. Gay, Parker, S. Jr., *The New Basement Tectonics*, 1972.
21. Garfunkel, Z., *Math. Phys. Sci.*, 1989, **254**, 181–208.
22. Nur, A., Ron, H. and Scott, O., *Palaeomagnetic Rotations and Continental Deformation*, Kluwer, Academic Publishers, Dordrecht, 1989.

ACKNOWLEDGEMENTS. We thank Dr T. M. Mahadevan for his encouragement and suggestions during the course of this work. We appreciate the neat drawings by John Andrews, G. Ramachandra Rao and B. Vyaghreswarudu. Sri A. Lingiah and G. D. P. Sitarama Sinha have digitised the data and prepared the required data base.

Received 8 July 1996; revised accepted 15 January 1997

Statistical analysis of glaciers in Himachal Pradesh, north-west Himalaya, India

D. P. Dobhal and Surendar Kumar

Wadia Institute of Himalayan Geology, Dehradun 248 001, India

A statistical analysis of Himachal glaciers has been carried out. The maximum concentration of glaciers is in the elevation range 4500–5500 m. More glaciers are of transverse simple type than longitudinal type.

THE Himalaya, on the southern slopes of the Tibetan plateau, is one of the most important glacier systems on the earth. The main snow-gathering ground is in the higher Greater Himalayan ranges, whose relationship with climate changes on various time scales indicates topographic and climatic conditions favourable for the formation of the glaciers. The present work is in continuation of our glacier inventory[1].

The study area is situated in the western part of the Himalaya, extending about 315 km between UP Himalaya in the east and the Kashmir Himalaya in the west (Figure 1). It encompasses mountain area of about 48,034 km^2 out of the total land area of 55,673 km^2 of the Himachal Himalaya. It is estimated that 9.4% (approximate 10%) is glaciated area of 4516.22 km^2 out of the total mountainous area of 48,034 km^2. Every 1 km^2 of the land area is glaciated to the extent of 0.09 km^2. Six hundred one glaciers have been identified in six drainage basins[2], Chandra–Bhaga (200), Beas–Parbati (80), Ravi (54), Malung (40), Spiti (159) and Satluj (68). Statistical analysis of glaciers in these drainage basins has been carried out on the basis of earlier works[2–8].

Glaciers are unevenly distributed between the Great Himalayan, Pir-Panjal and Dhauladhar ranges, controlled by the topographic variation and the amount of precipitation in the region. The altitude increases from NW to SE, where maximum precipitation occurs. So, the Satluj basin, which receives more precipitation and is at higher elevation, remains covered with snow for longer duration than the other basins. In this study the identification of glaciers is from LANDSAT imagery. Data for the glaciers are summarized in Tables 1 and 2.

In Chandra–Bhaga, Spiti and Satluj basins the highest frequency of glaciers is in the length range 2–4 km, while in Beas–Parbati, Ravi and Malung basins the highest frequency is around 2 km (Figure 2 *a*). It is also observed that 35% of the glaciers fall in the range 2–4 km in length, 55% are around 5 km, and the remaining 10% are 10 km or more in length. Bara-Shigri is the longest glacier (29 km) of the Himachal Himalaya.

The area covered by individual glaciers was calculated by digital planimeter. Figure 2 *b* shows that majority of the glacial cover area of Himachal extends over 2 to 6 km^2, but some glaciers are more than 10 km^2 in area. An examination of Table 1 shows that the Chandra–Bhaga, Malung and Spiti basins are relatively balanced in basin area and glaciated area, while the Beas, Ravi and Satluj are less glaciated compared to the basin area. The glaciers in NW Himachal Pradesh are bigger than those in the SE region.

Broadly the glaciers have been classified into two main types (i) Longitudinal and (ii) Transverse, on the basis of their flow direction[3]. These are further subdivided into simple and compound types. Simple glaciers have a single accumulation zone while compound glaciers have two or more accumulation zones in a single basin.